Direct Observation of the Transition from Calcite to Aragonite Growth as Induced by Abalone Shell Proteins

James B. Thompson,* George T. Paloczi,* Johannes H. Kindt,* Martina Michenfelder,† Bettye L. Smith,*† Galen Stucky,‡ Daniel E. Morse,†and Paul K. Hansma*

*Department of Physics, †Department of Molecular, Cellular and Developmental Biology, and ‡Department of Chemistry, University of California Santa Barbara, Santa Barbara, California 93106 USA

ABSTRACT The mixture of EDTA-soluble proteins found in abalone nacre are known to cause the nucleation and growth of aragonite on calcite seed crystals in supersaturated solutions of calcium carbonate. Past atomic force microscope studies of the interaction of these proteins with calcite crystals did not observe this transition because no information about the crystal polymorph on the surface was obtained. Here we have used the atomic force microscope to directly observe changes in the atomic lattice on a calcite seed crystal after the introduction of abalone shell proteins. The observed changes are consistent with a transition to (001) aragonite growth on a (1014) calcite surface.

INTRODUCTION

Abalone shells contain two distinct polymorphs of calcium carbonate. The outer portion of the shell consists of calcite, whereas the inner portion of the shell (nacre) consists of aragonite (Wada, 1961; Watabe and Wilbur, 1976; Nakahara et al., 1982; Jackson et al., 1988; Heuer et al., 1992; Sarikaya, 1994; Zaremba et al., 1996). In flat pearls deposited on inorganic substrates implanted near abalone shell-forming tissues, the transition from calcite to aragonite was observed to occur abruptly, without the apparent intervention of a nucleating organic matrix (Fritz et al., 1994; Zaremba et al., 1996). Previous studies have shown that the mixture of soluble proteins found in abalone nacre cause the nucleation and growth of aragonite needles on the (1014) faces of calcite seed crystals in supersaturated calcium carbonate solutions (Belcher et al., 1996). Similar control of calcium carbonate polymorph has also been reported for soluble proteins extracted from other mollusk species (Falini et al., 1996; Samata et al., 1999; Kono et al., 2000). Furthermore, soluble proteins associated with a variety of calcium carbonate biominerals have been shown to interact with calcite growth, become occluded within calcite crystals, and affect a variety of crystal properties (Berman et al., 1988, 1993; Didymus et al., 1993; Wierzbicki et al., 1994; Aizenberg et al., 1994; Sims et al., 1995; Belcher et al., 1996; Falini et al., 1996). Previously, the atomic force microscope (AFM) (Binnig et al., 1986) has been used to study crystal growth in situ (Malkin et al., 1995; Paloczi et al., 1998; Teng et al., 1998; Land et al., 1999) and to observe the atomic lattice of calcite (Hillner et al., 1992; Ohnesorge and Binnig, 1993; Stipp et al., 1994; Liang et al., 1996) as well as other biominerals (Siperko and Landis, 1992). In particular, proteins isolated from abalone nacre were shown to affect the shape of calcite growth steps and roughen the calcite surface (Walters et al., 1997). However, these studies did not allow the identification of the calcium carbonate polymorph present on the surface. Here we show that the AFM can directly observe changes in the surface lattice of a growing calcite crystal in the presence of abalone shell proteins. The observed changes in crystal lattice are correlated to the known crystal structures of calcite and aragonite.

MATERIALS AND METHODS

Calcium carbonate growth solutions were prepared following established procedures (Walters et al., 1997). Appropriate amounts of $CaCl_2$ and NaCl were added to one beaker and $NaHCO_3$ to another. Purified water (Milli-Q; Millipore Systems, Bedford, MA) was added to each beaker so that each contained slightly less than half the final volume. After mixing each beaker separately they were mixed together, and additional purified water was added to reach the desired final volume. The pH of the resulting solution was adjusted up to 8.1 by adding a few drops of 25 mM NaOH. The resulting solutions had final concentrations of 0.5 M sodium chloride, 4 mM calcium, and 4 mM total carbonate. These solutions were estimated to be 3.1X supersaturated at 25°C using the Geochemist's Workbench computer program. Fresh calcium carbonate growth solutions were prepared each day and stored in sealed containers. The pH of the solutions was reconfirmed before use. All solutions were prepared using reagent-grade $CaCl_2$, $NaHCO_3$, NaCl, and NaOH (Fisher, Fair Lawn, NJ).

To prepare the proteins used in this experiment, the prismatic calcite on the outer side of the red abalone (*Haliotis rufescens*) shell was removed from the nacre (aragonite) with a bead blaster. The nacre was then ground in a shatter box, and x-ray diffraction was used to ensure the purity of the mineral phase. Ten grams of this aragonite powder were demineralized with 0.5 M EDTA (pH 8.0) overnight. After centrifugation and separation from the EDTA-insoluble material, the supernatant was dialyzed exhaustively against water and then lyophilized (Cariolou and Morse, 1988). The lyophilized protein mixture was dissolved in 50 mM Tris-HCl buffer (pH 8.0) to a protein concentration of 2 mg/ml. The resulting protein concentrate was kept frozen at −80°C. Just before use, the protein concentrate would be thawed and diluted to a protein concentration of 2 μg/ml in the calcium carbonate growth solution described above.

Received for publication 30 May 2000 and in final form 13 September 2000.

G. T. Paloczi's present address: Department of Physics, California Institute of Technology, Pasadena, CA 91125.

Address reprint requests to Dr. James B. Thompson, Physics Department, University of California, Santa Barbara, CA 93106. Tel.: 805-893-3999; Fax: 805-893-8315; E-mail: jbthomp@physics.ucsb.edu.

0006-3495/00/12/3307/06 $2.00

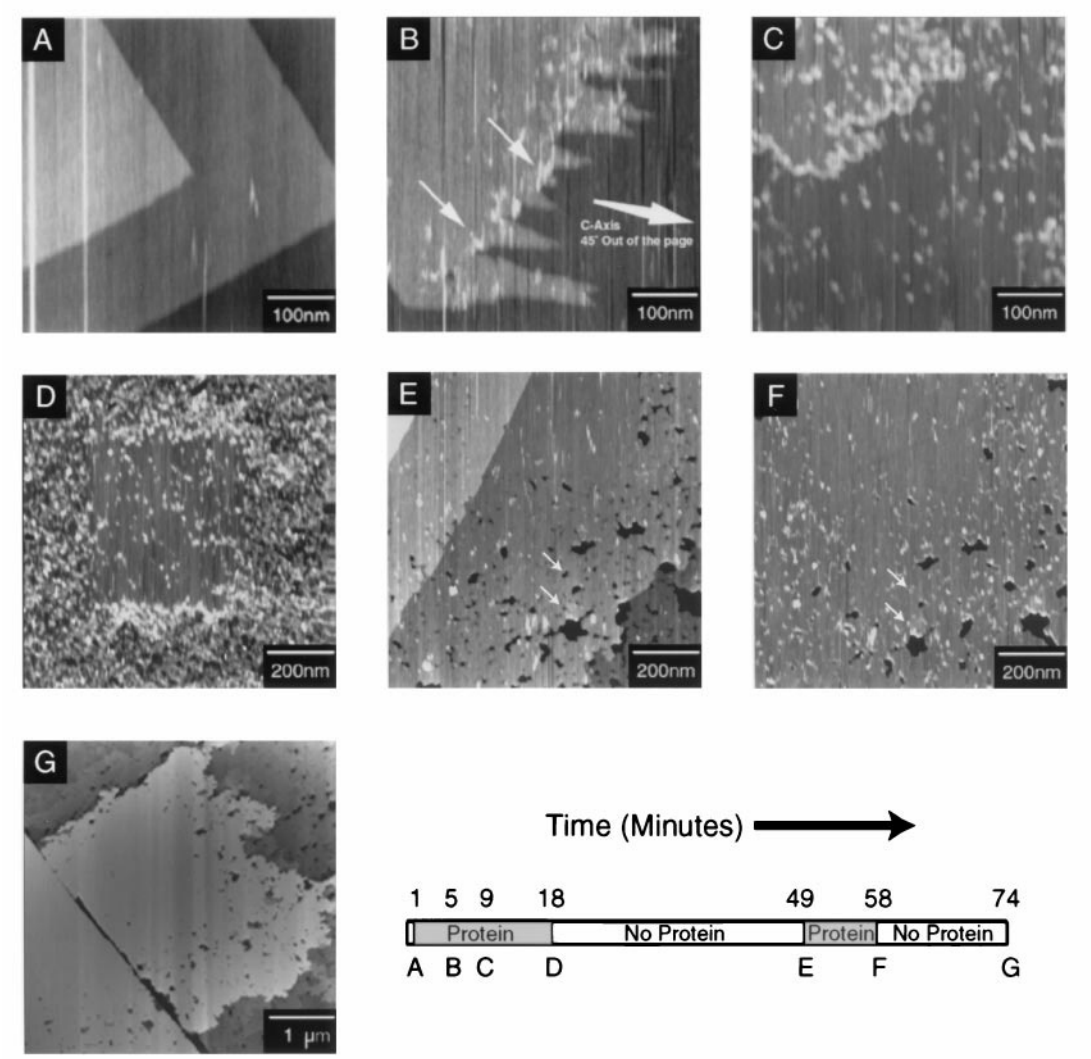

FIGURE 1 Calcite (10$\underline{1}$4) cleavage plane before and after the introduction of soluble abalone nacre proteins. (*A*) Before the introduction of proteins we observe straight 0.3-nm calcite growth steps. (*B*) The arrows indicate the points where proteins interact with and retard the progress of the step edge. As indicated in the figure, the *c*-axis of the calcite seed crystal is 45° out of the page. All of the images presented in the paper have the same orientation of the *c*-axis. (*C*) A step edge can be seen in the upper left quadrant of the picture, but now it is completely covered with proteins. The observed step velocity becomes greatly reduced. (*D*) After imaging in the same area for 18 min, we zoomed out to a 1-μm scan range. Outside of the original scan area the crystal has become littered with proteins. It appears that the AFM either removed or prevented the attachment of material inside its scan area. (*E*) In the absence of proteins, the surface becomes smoother. After 30 min, step growth resumes. (*F*) Once again, the surface is exposed to proteins. After a few minutes, no more growth steps appeared on the surface, and many pits in the surface became filled with proteins (*arrows*). (*G*) A relatively large area scan shows that the surface has become smooth, in the absence of proteins, even in areas where the AFM has not previously scanned. The timeline denotes when each image was taken and when we switched between calcium carbonate growth solution with or without proteins.

The (1014) calcite surfaces used in this experiment were prepared, as needed, by attaching a calcite crystal (Ward's Earth Science, Rochester, NY) to a disk of magnetic stainless steel with hot melt epoxy (Epon; Shell, Houston, TX). The crystals were then scribed with a razor blade and cleaved. The freshly cleaved surface was covered with calcium carbonate growth solution to prevent contamination (Walters et al., 1997).

The images presented in this paper were taken using a commercial AFM (MultiMode; Digital Instruments, Santa Barbara, CA) and cantilevers (180-μm-long Contact Ultralevers; Park Scientific, Palo Alto, CA) in contact mode. During imaging, the solution in contact with the sample was constantly exchanged using a home-built gravity feed system so that the sample would not cause dramatic changes to the solution chemistry. The ~20-μl fluid cell volume was replaced at a rate of approximately 7 μl/s. It was possible to switch between solutions containing proteins and those without proteins during the course of the experiment.

The images whose scan ranges vary from 0.5 to 5 μm were taken at scan rates of 10 Hz with 256 lines per image for an image acquisition time of 26 s. The lattice resolution images were taken at scan rates of 36 Hz with 256 lines per image for an image acquisition time of 7 s. We found that high scan rates, high gain settings, minimal imaging force, and fortuitously sharp AFM tips yielded the best lattice resolution images. Unfortunately, the last of these requirements was not under our control. We simply had to try several tips to find one that was satisfactory. The structure seen in the lattice resolution images was seen in both up and down scans. And the

observed lattice spacings are the averages of measurements made on both up and down scans to mitigate the effect of sample drift.

To make the interpretation of our lattice resolution data easier and more intuitive, we have added false color to the images using custom image analysis software developed in our lab. The software adds false color to AFM images according to which portions of the image contribute to certain peaks in the image's reciprocal space representation. The software starts with an ASCII data file (We exported our images using the ASCII export utility in the Nanoscope III software package; Digital Instruments) and performs a two-dimensional Fourier transform to produce a reciprocal space representation. The user then selects a region around each of two peaks in reciprocal space. The software performs an inverse transform on each of the selected regions and rectifies the result to get the amplitude of each periodicity in various parts of the image. The software creates a color map that shows which regions of the surface are dominated by each periodicity. The resulting color map is combined with the height data, which is displayed as brightness in the images. Because the data extracted from the Fourier transform affects the color, but not the brightness of the image, printing the image on a black and white printer simply yields the raw data. The software used to process our lattice images can be downloaded from http://hansmalab.physics.ucsb.edu/latticepaint/.

The molecular model of aragonite was prepared using the solids builder in Insight II (Molecular Simulations, San Diego, CA).

RESULTS

When we imaged a freshly cleaved calcite crystal under a calcium carbonate growth solution, we saw 0.3-nm calcite growth steps across the entire surface (see Fig. 1 *A*). The calcite steps proceed at different speeds in different crystallographic directions, enabling us to determine the in-plane orientation of our sample (Gratz et al., 1993).

Once we switched to a growth solution supplemented with the mixture of soluble proteins found in abalone nacre (see Materials and Methods), we observed morphological alterations of the surface as previously demonstrated by Walters et al. (1997). Fig. 1 shows representative images of the effects of abalone shell proteins on growing calcite. As expected, we observed a roughening of the step edges and cessation of crystal growth. Closer observation shows that individual proteins impeded the progress of the growth step at the point of their attachment and moved with the step edge (Fig. 1 *B*). This resulted in the jagged appearance of the step edges and correlates with step rounding seen in other studies (Walters et al., 1997). Eventually, the surface became littered with proteins, but the AFM removed much of this material in the region where it had been scanning for the previous 18 min (Fig. 1 *D*). In the absence of protein-supplemented solution the surface regained a smooth appearance and step growth resumed (Fig. 1 *E*). At this point we switched back to the protein-supplemented solution. After nine additional minutes of exposure to the protein solution, step growth stopped (Fig. 1 *F*). The surface was now largely smooth, even in areas where the AFM had not previously imaged (Fig. 1 *G*).

We studied these surfaces at much higher resolution to determine whether the lattice structure on the surface changed in response to the addition of abalone shell pro-

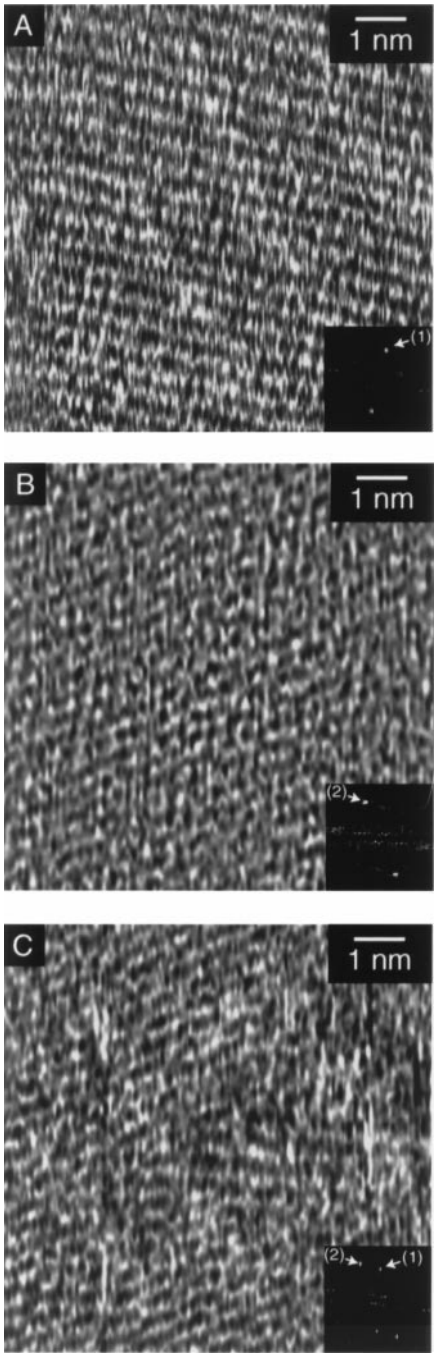

FIGURE 2 Lattice resolution images of the surface before and after the introduction of soluble proteins extracted from abalone nacre. All of these images were taken on the same sample without rotating the sample or the scan angle. (*A*) The first image shows the calcite (10$\underline{1}$4) surface before the introduction of abalone proteins. The inset is a reciprocal space representation of the image. The primary peak in reciprocal space (1) corresponds to the 0.50-nm lattice spacing of calcite. Before the introduction of proteins the surface lattice exhibits a uniform appearance in all areas that we imaged. (*B*) After the introduction of proteins the surface lattice appears to be altered. The reciprocal space representation shows a different peak (2) that corresponds to a periodicity of 0.41 nm. (*C*) After the introduction of proteins, the surface lattice appears disturbed in some areas. The reciprocal space representation contains both peaks (1) and (2), indicating that both of the previously observed lattice spacings are present in this image.

teins. Before the introduction of abalone shell proteins, we see lines or rows on the surface spaced 0.5 nm apart, which is consistent with results seen elsewhere for the (10$\underline{1}$4) surface of calcite (Fig. 2 *A*) (Hillner et al., 1992; Ohnesorge and Binnig, 1993; Stipp et al., 1994; Liang et al., 1996). These rows are aligned with the *c*-axis of the calcite crystal, and the spacing between them corresponds to the lattice spacing on the calcite (10$\underline{1}$4) surface perpendicular to the *c*-axis. After the introduction of proteins, much of the surface exhibits a different lattice structure that is rotated from the first and has a smaller lattice spacing (Fig. 2 *B*). In other regions, the lattice does not have a uniform appearance. In Fig. 2 *C*, it appears that two different lattices are present on the surface.

The observed change in lattice structure is apparent in reciprocal space (see insets in Fig. 2). The inset in Fig. 2 *A* (a two-dimensional Fourier transformation of the image) shows a dominant peak that corresponds to a 0.5-nm lattice spacing. The inset in Fig. 2 *B* contains a totally different peak, indicating that the surface lattice has changed. The inset in Fig. 3 *C*, however, shows both peaks, suggesting that both lattice structures are present in the image.

To determine which areas in each image contributed to the observed peaks in reciprocal space, we processed the images using a custom software package. The software added false color to reflect the contribution that any given part of the surface made to a small region surrounding each of the two dominant peaks in reciprocal space (see Materials and Methods). All three images in Fig. 2 were analyzed in this fashion, without changing the selected regions in reciprocal space.

After processing the images, we see that Fig. 3, *A* and *B*, primarily contain only one of the two observed lattice spacings, whereas Fig. 3 *C* contains two distinct areas. The coloration of Fig. 3 *C* shows that the lattice spacing observed in each of these areas contributes to the selected regions of reciprocal space in the same proportion as the lattices observed in Fig. 3, *A* and *B*. Some areas in the images are not consistent with either lattice spacing. These areas appear gray in Fig. 3 and may represent defects in the crystalline surface.

DISCUSSION

Fig. 3 *D* shows the location of the calcium atoms on both the (001) aragonite and (10$\underline{1}$4) calcite surfaces as predicted from the bulk crystal structure of each material. The surface

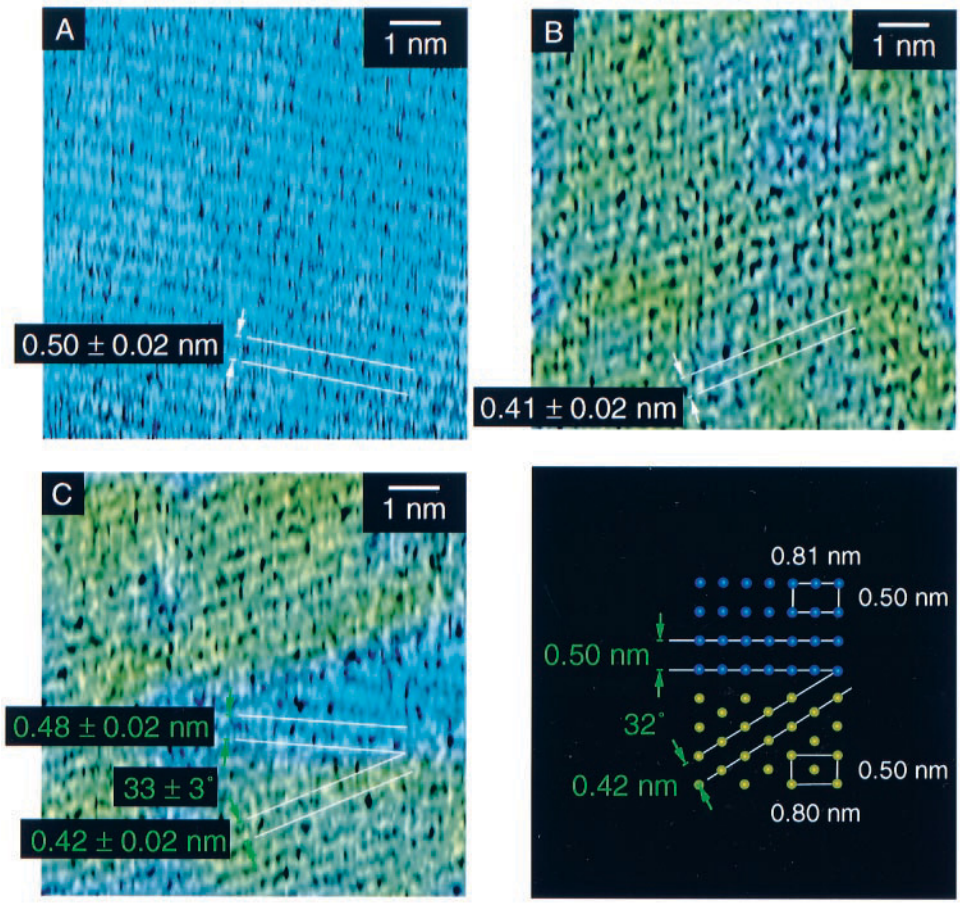

FIGURE 3 Lattice resolution images of the surface before and after the introduction of soluble proteins extracted from abalone nacre. The images are colorized according to the contribution that each part of the image makes to a certain peak in reciprocal space. (*A* and *B*) These images primarily contribute to only one of the two observed peaks in reciprocal space. (*C*) In this image, we see two distinct areas. Each area corresponds to one of the lattice structures observed in *A* or *B*. (*D*) The calcium surface lattices of the calcite (10$\underline{1}$4) cleavage plane (*upper*, violet atoms) and aragonite (001) plane (*lower*, yellow atoms) as they would appear if they were on the same surface with their unit cells aligned. This is a likely orientation for aragonite grown on calcite due to the similarity of the surface unit cells. In the AFM, the surface lattice frequently appears as lines that join neighboring surface atoms. Lines that join nearest neighbors on these surfaces are rotated by 32° with respect to one another. The line spacings as well as the relative orientation of the lines predicted in this model match those measured from Fig. 2, *B* and *C*, suggesting that the observed changes in lattice structure are consistent with a transition to (001) aragonite growth.

unit cells of these two materials are extremely similar. This similarity seems to indicate that growing (001) aragonite on a (10$\underline{1}$4) calcite surface, while maintaining long-range order at their interfaces, would require that the surface unit cells be in angular alignment. If we take this to be true, then the two surface lattices might lay side by side on a surface as they are shown in Fig. 3 *D*.

From the model in Fig. 3 *D*, we can predict the lattice spacings we would observe with the AFM, as well as the angle between the two lattices. The AFM does not usually attain true atomic resolution because AFM tips are not, generally, atomically sharp (Gould et al., 1989). However, one can often observe one or more of the lattice spacings on a surface as shown here. Frequently, the observed lattice spacings correspond to the distance between lines that connect the nearest neighboring atoms on a crystalline surface (Hillner et al., 1992). For (10$\underline{1}$4) calcite, such lines are 0.50 nm apart, which corresponds to the shorter of its surface lattice parameters. For (001) aragonite, the surface lattice is nearly but not quite hexagonal, and the distance between any two nearest neighbors on the surface is 0.46 nm. The distance between two lines drawn as those in the lower half of Fig. 3 *D* is then 0.42 nm, and those lines form an angle of 32° with the calcite lattice.

The lattice spacings and angles predicted by the model are in excellent agreement with the measurements shown in Fig. 3, *A–C*, suggesting that the observed change in lattice structure is consistent with the transition from calcite to aragonite growth that has been observed in bulk samples (Belcher et al., 1996). These observations support the earlier suggestions (Fritz et al., 1994; Zaremba et al., 1996; Belcher et al., 1996) that the transition from calcite to aragonite can be induced by the addition of soluble proteins extracted from the abalone shell nacre (aragonite), without the need for nucleation on a preformed organic matrix. However, the AFM data alone cannot positively identify the second crystal structure we observe, as the (001) surface lattices of calcite and vaterite are similar to that of (001) aragonite.

The ability to observe a change in surface structure so early in its development may be unique to scanning probe techniques, as they are by their nature insensitive to material below the surface of the sample. As a result, the bulk structure of the sample does not provide a background signal as it might with diffraction techniques. Furthermore, scanning probe techniques allow the study of local changes, or defects, in lattice structure such as the one seen in Fig. 3 *C*, where there appears to be a calcite defect in an aragonite layer. Combining these features with the AFM's ability to image organic macromolecules such as proteins under physiologically relevant conditions makes the AFM uniquely suited to study biological control of inorganic materials. In particular, we intend to extend our work to hydroxyapatite biominerals such as teeth (Margolis et al., 1999; Simmer et al., 1998; Snead, 1996; Fong et al., 2000; White et al., 2000).

We thank Paul Levine, Chris Brown, Deron Walters, Tilman Shäffer, and Mario Viani for useful discussion.

This work was supported by the Army Research Office, MURI Program (grant DAAH04–96-1–0443), the Office of Naval Research (grant N00014–93-10584), the Materials Research Laboratory Program of the National Science Foundation (grant DMR-9632716), and the National Science Foundation (grant DMR-9622169). The U.S. Government is authorized to reproduce and distribute copies for governmental purposes.

REFERENCES

Aizenberg, J., S. Albeck, S. Weiner, and L. Addadi. 1994. Crystal-protein interactions studied by overgrowth of calcite on biogenic skeletal elements. *J. Cryst. Growth.* 142:156–164.

Belcher, A. M., X. H. Wu, R. J. Christensen, P. K. Hansma, G. D. Stucky, and D. E. Morse. 1996. Control of crystal phase switching and orientation by soluble mollusc-shell proteins. *Nature.* 381:56–58.

Berman, A., L. Addadi, and S. Weiner. 1988. Interactions of sea-urchin skeleton macromolecules with growing calcite crystals: a study of intracrystalline proteins. *Nature.* 331:546–548.

Berman, A., H. Hanson, L. Leiserowitz, T. F. Koetzle, S. Weiner, and L. Addadi. 1993. Biological control of crystal texture: a widespread strategy for adapting crystal properties to function. *Science.* 259:776–779.

Binnig, G., C. F. Quate, and C. Gerber. 1986. Atomic force microscope. *Phys. Rev. Lett.* 56:930–933.

Cariolou, M. A., and D. E. Morse. 1988. Purification and characterization of calcium-binding conchiolin shell peptides from the mollusc, *Haliotis rufescens*, as a function of development. *J. Comp. Physiol. B.* 157: 717–729.

Didymus, J. M., P. Oliver, S. Mann, A. L. Devries, P. V. Hauschka, and P. Westbroek. 1993. Influence of low-molecular-weight and macromolecular organic additives on the morphology of calcium carbonate. *J. Chem. Soc. Faraday Trans.* 89:2891–2900.

Falini, G., S. Albeck, S. Weiner, and L. Addadi. 1996. Control of aragonite polymorphism by mollusk shell macromolecules. *Science.* 271:67–69.

Fong, H., M. Sarikaya, S. N. White, and M. L. Snead. 2000. Nanomechanical properties profiles across dentin-enamel junction of human incisor teeth. *Mat. Sci. Eng. C-Bio. S.* 7:119–128.

Fritz, M., A. M. Belcher, M. Radmacher, D. A. Walters, P. K. Hansma, G. D. Stucky, D. E. Morse, and S. Mann. 1994. Flat pearls from biofabrication of organized composites on inorganic substrates. *Nature.* 371:49–51.

Gould, S. A. C., K. Burke, and P. K. Hansma. 1989. Simple theory for the atomic-force microscope with a comparison of theoretical and experimental images of graphite. *Phys. Rev. B.* 40:5363–5366.

Gratz, A. J., P. E. Hillner, and P. K. Hansma. 1993. Step dynamics and spiral growth on calcite. *Geochim. Cosmochim. Acta.* 57:491–495.

Heuer, A. H., D. J. Fink, V. J. Laraia, J. L. Arias, P. D. Calvert, K. Kendall, G. L. Messing, J. Blackwell, P. C. Rieke, D. H. Thompson, A. P. Wheeler, A. Veis, and A. I. Caplan. 1992. Innovative materials processing strategies: a biomimetic approach. *Science.* 255:1098–1105.

Hillner, P. E., A. J. Gratz, S. Manne, and P. K. Hansma. 1992. Atomic-scale imaging of calcite growth and dissolution in real time. *Geology.* 20:359–362.

Jackson, A. P., J. F. V. Vincent, and R. M. Turner. 1988. The mechanical design of nacre. *Proc. R. Soc. Lond. B Biol. Sci.* 234:415–440.

Kono, M., N. Hayashi, and T. Samata. 2000. Molecular mechanism of the nacreous layer formation in *Pinctada maxima*. *Biochem. Bioph. Res. Commun.* 269:213–218.

Land, T. A., T. L. Martin, S. Potapenko, G. T. Palmore, and J. J. De Yoreo. 1999. Recovery of surfaces from impurity poisoning during crystal growth. *Nature.* 399:442–445.

Liang, Y., A. S. Lea, D. R. Baer, and M. H. Engelhard. 1996. Structure of the cleaved $CaCO_3$ (1014) surface in an aqueous environment. *Surf. Sci.* 351:172–82.

Malkin, A. J., T. A. Land, Y. G. Kuznetsov, A. McPherson, and J. J. DeYoreo. 1995. Investigation of virus crystal growth mechanisms by in situ atomic force microscopy. *Phys. Rev. Lett.* 75:2778–2781.

Margolis, H. C., Y. P. Zhang, C. Y. Lee, R. L. Kent, and E. C. Moreno. 1999. Kinetics of enamel demineralization in vitro. *J. Dent. Res.* 78: 1326–1335.

Nakahara, H., G. Bevelander, and M. Kakei. 1982. Electron microscope and amino acid studies on the outer and inner shell layers of *Haliotis rufescens*. *Venus Jap. J. Malac.* 41:33–46.

Ohnesorge, F., and G. Binnig. 1993. True atomic-resolution by atomic force microscopy through repulsive and attractive forces. *Science.* 260: 1451–1456.

Paloczi, G. T., B. L. Smith, P. K. Hansma, D. A. Walters, and M. A. Wendman. 1998. Rapid imaging of calcite crystal growth using atomic force microscopy with small cantilevers. *Appl. Phys. Lett.* 73: 1658–1660.

Samata, T., N. Hayashi, M. Kono, K. Hasegawa, C. Horita, and S. Akera. 1999. A new matrix protein family related to the nacreous layer formation of *Pinctada fucata*. *Febs Lett.* 462:225–229.

Sarikaya, M. 1994. An introduction to biomimetics: a structural viewpoint. *Microsc. Res. Techniq.* 27:360–375.

Simmer, J. P., M. Fukae, T. Tanabe, Y. Yamakoshi, T. Uchida, J. Xue, H. C. Margolis, M. Shimizu, B. C. DeHart, C. C. Hu, and J. D. Bartlett. 1998. Purification, characterization, and cloning of enamel matrix serine proteinase 1. *J. Dent. Res.* 77:377–386.

Sims, S. D., J. M. Didymus, and S. Mann. 1995. Habit modification in synthetic crystals of aragonite and vaterite. *J. Chem. Soc. Chem. Commun.*1031–1032.

Siperko, L. M., and W. J. Landis. 1992. Atomic scale imaging of hydroxyapatite and brushite in air by force microscopy. *Appl. Phys. Lett.* 61: 2610–2612.

Snead, M. L. 1996. Enamel biology logodaedaly: getting to the root of the problem, or who's on first. *J. Bone Miner. Res.* 11:899–904.

Stipp, S. L. S., C. M. Eggleston, and B. S. Nielsen. 1994. Calcite surface structure observed at microtopographic and molecular scales with atomic force microscopy (AFM). *Geochim. Cosmochim. Acta.* 58: 3023–3033.

Teng, H. H., P. M. Dove, C. A. Orme, and J. J. De Yoreo. 1998. Thermodynamics of calcite growth: baseline for understanding biomineral formation. *Science.* 282:724–727.

Wada, K. 1961. Crystal growth of molluscan shells. *Bull. Natl. Pearl Res. Lab.* 7:703–828.

Walters, D. A., B. L. Smith, A. M. Belcher, G. T. Paloczi, G. D. Stucky, D. E. Morse, and P. K. Hansma. 1997. Modification of calcite crystal growth by abalone shell proteins: an atomic force microscope study. *Biophys. J.* 72:1425–33.

Watabe, N., and K. M. Wilbur. 1976. The Mechanisms of Biomineralization in Invertebrates and Plants. University of South Carolina Press, Columbia, SC. 283–308.

White, S. N., M. L. Paine, W. Luo, M. Sarikaya, H. Fong, Z. K. Yu, Z. C. Li, and M. L. Snead. 2000. The dentino-enamel junction is a broad transitional zone uniting dissimilar bioceramic composites. *J. Am. Ceram. Soc.* 83:238–240.

Wierzbicki, A., C. S. Sikes, J. D. Madura, and B. Drake. 1994. Atomic force microscopy and molecular modeling of protein and peptide binding to calcite. *Calc. Tissue Int.* 54:133–141.

Zaremba, C., A. M. Belcher, M. Fritz, Y. Li, S. Mann, P. K. Hansma, D. E. Morse, J. S. Speck, and G. D. Stucky. 1996. Critical transitions in the biofabrication of abalone shells and flat pearls. *Chem. Mater.* 8:679–690.